Chemical Science

ROYAL SOCIETY OF CHEMISTRY

EDGE ARTICLE

View Article Online
View Journal | View Issue

Cite this: *Chem. Sci.*, 2025, **16**, 4703

All publication charges for this article have been paid for by the Royal Society of Chemistry

Synergistic engineering of ultraviolet metal-free crystals with exceptional birefringence *via* pyridine-derived dimers†

Jiachen Lu and Kang Min Ok *

Crystals with giant birefringence are essential for practical applications in lasers, optical communication, and polarimetry, where precise control of polarized light is critical. Coplanar six-membered ring (6-MR) primitives with large polarizability anisotropy are particularly effective in enhancing birefringence. This study successfully combines different pyridine derivatives into two novel metal-free crystals: supramolecular one-dimensional [(4-HP)(4-H_2P)][3-pSO_3] (**1**; HP = hydroxypyridine; py = pyridine) and two-dimensional [4-AP][3-pSO_3] (**2**; AP = aminopyridne), synthesized *via* a facile aqueous solution method. Compound **1** features unique [4-HP/4-H_2P]$^+$ cationic dimer pairs linked by hydrogen bonds, in contrast to the single monovalent [4-AP]$^+$ cations in compound **2**. This structural distinction leads to optimized anionic [3-pSO_3]$^-$ arrangements, a reduced dimensionality of linkage, and denser spatial distribution of cationic pseudo-layers, significantly enhancing birefringence. Compound **1** exhibits a superior birefringence value of 0.443 at 546 nm, compared to 0.296 for compound **2**, representing the highest birefringence among sulfate derivatives incorporating an additional birefringence-active group in the ultraviolet (UV) region. It also surpasses all reported metal-free compounds with single 6-MRs in the short-wave UV range. Theoretical calculations confirm the synergistic effects between cationic and anionic pyridine derivatives, further elucidating their contributions to enhanced birefringence. In addition, compound **1** demonstrates a short UV cut-off edge at 279 nm and favorable growth characteristics, making it a promising candidate for UV birefringent applications. This research offers new insights into designing and optimizing birefringence by exploring the relationship between the composition and arrangement of organic cations and their optical properties in UV metal-free systems through synergistic effects.

Received 7th January 2025
Accepted 5th February 2025

DOI: 10.1039/d5sc00112a

rsc.li/chemical-science

Introduction

Birefringent crystals, particularly those with high birefringence values (Δn), are critical for applications such as lasers, optical communication, and polarimetry attributable to their ability to regulate polarized light.[1–6] Although several birefringent materials, including YVO_4 (Δn = 0.225 @633 nm), α-BaB_2O_4 (Δn = 0.122 @532 nm), $LiNbO_3$ (0.074 @546 nm), and TiO_2 (Δn = 0.305 @546 nm), have been commercialized, these materials face inherent limitations.[7–10] Challenges such as high-temperature crystallization and the elevated production costs associated with expensive metal elements (*e.g.*, niobium and lithium in $LiNbO_3$) restrict their widespread application.[11–14] Consequently, attention has shifted to crystals composed solely of light elements (*e.g.*, C, B, N, H, O, F, S), which offer the advantages of facile synthesis *via* aqueous solution methods.[15–17] This approach presents significant opportunities for developing promising candidates with large birefringence within metal-free systems.

A promising strategy for designing novel metal-free crystals with high birefringence involves combining birefringence-active cationic and anionic groups generated through protonation and deprotonation. Examples include compounds such as $C(NH_2)_3BF_4$,[18] $[C_3N_6H_7]_2[B_3O_3F_4(OH)]$,[19] and others.[20–23] The synergistic effects of these groups, facilitated by optimal structural arrangements, can lead to substantial birefringence enhancement. Hydrogen bonding is frequently employed to link these birefringence-active groups (BAGs), thereby influencing both the structural and optical properties. For instance, Pan *et al.* achieved a birefringence of 0.371 @532 nm,

Department of Chemistry, Sogang University, Seoul 04107, Republic of Korea. E-mail: kmok@sogang.ac.kr

† Electronic supplementary information (ESI) available: Crystallographic data, PXRD patterns, IR spectra, TGA diagrams, experimental and calculated band gaps, ELF diagrams, thickness of crystals for birefringence measurements for compounds **1** and **2**, comparison of experimental birefringence among metal-free compounds containing single 6-MRs in the short-wave UV region, comparison of experimental birefringence among UV sulfate derivatives incorporating an additional BAG, and birefringence values for selected commercial birefringent crystals. CCDC 2393642 and 2393748. For ESI and crystallographic data in CIF or other electronic format see DOI: https://doi.org/10.1039/d5sc00112a

comparable to commercial materials, by linking π-conjugated $[C(NH_2)_3]^+$ and $[C_2O_3OH]^-$ units into mutually parallel but oppositely oriented $[C(NH_2)_3HC_2O_4]_\infty$ layers.[24]

To further optimize crystal structures, the density of BAGs has been explored. For example, $C_9H_7NBrNO_3$ incorporates a double six-membered ring (D6-MR) unit $[C_9H_6BrN]$ with high polarizability anisotropy ($\Delta\alpha$), combined with smaller π-conjugated $[NO_3]^-$ groups. These smaller units intercalate between parallel $[C_9H_7NBr]^+$ cations, achieving an ideal BAG density while maintaining a large $\Delta\alpha$, resulting in a birefringence of 0.564 @550 nm.[25] This highlights the effectiveness of densely packed 6-MRs, particularly those with exposed nitrogen atoms, as pyridine rings are known for their high polarizability anisotropy, which enhances birefringence.[26–30] Combining two pyridine-related units within a single structure through synergistic effects, rather than relying solely on larger D6-MR units, represents a promising strategy for designing birefringent crystals. Moreover, the frequent protonation of pyridine nitrogen atoms makes acidic groups ideal anionic sources for achieving charge balance.

Building on these insights, the sulfonic group (–SO_3H) was selected for this study, leading to the rational design and synthesis of two novel metal-free crystals: [(4-HP)(4-H_2P)][3-pySO_3] (**1**; HP = hydroxypyridine; py = pyridine) and [4-AP][3-pySO_3] (**2**; AP = aminopyridne). In these compounds, [4-HP/4-H_2P]$^+$ dimer pairs and single [4-AP]$^+$ cations are connected *via* hydrogen bond-based donor–acceptor systems, appearing in compounds **1** and **2**, respectively. These distinct cationic forms and functional groups influence the arrangement of [3-pySO_3]$^-$ anions, resulting in varying optical properties. Notably, compound **1** exhibits giant birefringence (0.443 @546 nm), the highest value reported among sulfate derivatives incorporating additional BAGs in the UV region. It also surpasses other metal-free compounds containing single 6-MRs in the short-wave UV range. Additionally, compound **1** features a short UV cut-off edge at 279 nm and favorable growth characteristics. The enhanced birefringence observed in compound **1** (0.296 → 0.443 @546 nm), as compared to compound **2**, is attributed to a denser distribution of cationic [4-HP/4-H_2P]$^+$ pseudo-layers and an optimized arrangement of [3-pySO_3]$^-$ anions. These findings provide valuable insights into the design and optimization of organic cations for achieving superior birefringence in UV metal-free systems through synergistic effects.

Experimental section

An aqueous solution method was employed for crystal growth. For compound **1**, 2 mmol of 3-pyridine sulfonic acid (98%, Alfa Aesar, 3-pySO_3H) and 4 mmol of 4-hydroxypyridine (>99%, TCI, 4-HP) were dissolved in 20 mL of H_2O and stirred at room temperature (RT) until a transparent solution was obtained. The solution was then evaporated in a Petri dish at RT, yielding plate-like yellow crystals after several days. For compound **2**, 4-HP was replaced with 2 mmol of 4-aminopyridine (98%, Alfa Aesar, 4-AP), resulting in plate-like, colorless crystals.

Powder X-ray diffraction (PXRD) measurements for compounds **1** and **2** were conducted using a MiniFlex 600 diffractometer equipped with Cu Kα radiation ($\lambda = 1.5406$ Å) at RT. The 2θ range was 5–70°, with a scan speed of 20° min^{-1} (Fig. 2a and S4†).

Thermogravimetric analysis (TGA) was performed using a SCINCO TGA-N 1000 thermal analyzer to obtain TGA spectra for compounds **1** and **2** (Fig. S6a and b†). Polycrystalline samples were placed in alumina crucibles and heated at a rate of 10 °C min^{-1} up to 900 °C under an air atmosphere.

Infrared (IR) spectra were recorded in the range of 650–4000 cm^{-1} using a Bruker TENSOR 27 ATR-FT-IR spectrometer (Fig. S5a and b†). A diamond attenuated total reflectance crystal was used to ensure direct contact with the ground samples for precise measurements.

UV-vis diffuse reflectance spectra for compounds **1** and **2** were acquired using a Lambda 1050 UV-vis spectrophotometer under ambient conditions across a spectral range of 200–800 nm (Fig. 2b).

The birefringence (Δn) at 546 nm for transparent crystals of compounds **1** and **2** was measured using a ZEISS Axiolab 5 polarizing microscope. The optical path difference (R) was determined using a Berek compensator, and birefringence was calculated using the equation $\Delta n = R/d$, where d represents the crystal thickness at the extinction position.

Single-crystal X-ray diffraction (SCXRD) data for compounds **1** and **2** were collected using a Bruker D8 QUEST diffractometer equipped with Mo Kα radiation ($\lambda = 0.71073$ Å) under ambient conditions at the Advanced Biointerface Core Facility, Sogang University. Data reduction was performed using the SAINT program, and absorption corrections were applied using the SADABS program.[31] Structural resolution and refinement were conducted using the OLEX2 program,[32] and higher symmetry was excluded using the PLATON program.[33] Crystallographic data and structure refinement details are provided in Table S1,† while atomic coordinates, bond lengths, bond angles, and hydrogen bond details are summarized in Tables S2–S6.†

First-principles calculations were carried out using the CASTEP package based on density-functional theory (DFT).[34] Simulated band structures, electron localization function (ELF), density of states (DOS), and optical properties for compounds **1** and **2** were computed using the Perdew–Burke–Ernzerhof (PBE) generalized gradient approximation (GGA) and norm-conserving pseudopotentials.[35–38] The pseudo-potential valence electrons were considered as follows: C-2$s^2$2p^2, N-2$s^2$2p^3, S-3$s^2$3p^4, O-2$s^2$2p^4, and H-1s^1. The plane-wave cut-off energy and dense k-point sampling were set to 830 eV and 0.03 Å^{-1}, respectively, with all other parameters set to ultra-fine defaults.

Results and discussion

SCXRD analysis revealed that compounds **1** and **2** crystallize in the $P2_1/c$ (No. 14) and *Pbcn* (No. 60) space groups, respectively (Tables S1–S6†). Compound **1** features a supramolecular one-dimensional (1D) chain structure (Fig. S1†), comprising infinite [(4-HP)(4-H_2P)][3-pySO_3] asymmetric units linked *via* N–H···O hydrogen bonds (Fig. 1a and b). Notably, both neutral [4-HP] and monovalent [4-H_2P]$^+$ coexist within the [(4-HP)(4-H_2P)][3-pySO_3] units. Consequently, [4-HP/4-H_2P]$^+$ dimer pairs

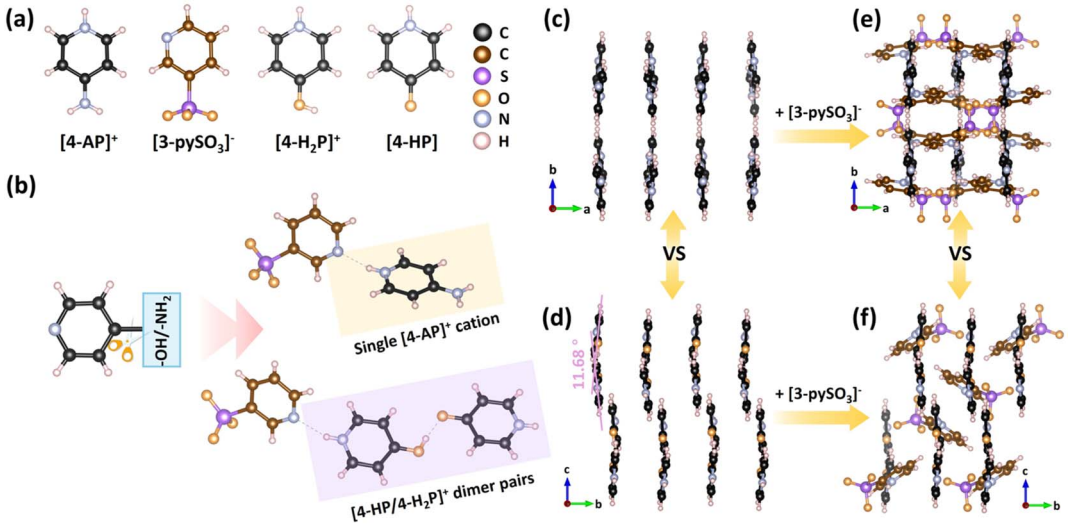

Fig. 1 (a) Functional modules: $[4\text{-AP}]^+$, $[3\text{-pySO}_3]^-$, $[4\text{-H}_2\text{P}]^+$, and neutral [4-HP]; (b) asymmetric units: $[(4\text{-HP})(4\text{-H}_2\text{P})][3\text{-pySO}_3]$ with $[4\text{-HP}/4\text{-H}_2\text{P}]^+$ dimer pairs in compound **1**, and $[4\text{-AP}/3\text{-pySO}_3]$ with a single $[4\text{-AP}]^+$ cation in compound **2**; (c) arrangement of $[4\text{-AP}]^+$ groups in compound **2**; (d) arrangement of $[4\text{-HP}/4\text{-H}_2\text{P}]^+$ dimer pairs in compound **1**; (e) arrangement of $[4\text{-AP}]^+$ and $[3\text{-pySO}_3]^-$ groups in compound **2**; (f) arrangement of $[4\text{-HP}/4\text{-H}_2\text{P}]^+$ and $[3\text{-pySO}_3]^-$ groups in compound **1**.

form through intermolecular hydrogen bonds in a donor–acceptor arrangement, functioning as a single cation. These dimers further combine anionic $[3\text{-pySO}_3]^-$ groups *via* N–H···N hydrogen bonds.

The small dihedral angle of 11.68° between the [4-HP] and $[4\text{-H}_2\text{P}]^+$ units facilitates a nearly parallel arrangement of the $[4\text{-HP}/4\text{-H}_2\text{P}]^+$ cationic pseudo-layers along the *ac* plane, significantly contributing to optical anisotropy (Fig. 1d).[39–41] Additionally, π–π interactions (centroid distances: 3.603–4.019 Å) between pyridine rings further stabilize the supramolecular 1D chains, forming the final structure of compound **1** (Fig. 1f and S3a†). In contrast, compound **2** adopts a supramolecular two-dimensional (2D) layered structure, $[4\text{-AP}(3\text{-pySO}_3)]_\infty$, oriented parallel to the *bc* plane (Fig. S2†). This structural difference arises from substituting the "–OH" group in compound **1** with an "–NH_2" group in compound **2**, which enables the formation of $[4\text{-AP}/3\text{-pySO}_3]$ dimers interconnected *via* N–H···O hydrogen bonds involving the amino and sulfonate groups. As a result, two oxygen atoms in the $[3\text{-pySO}_3]^-$ groups are simultaneously coordinated by these hydrogen bonds. The variation in hydrogen bonding influences the arrangement of anionic $[3\text{-pySO}_3]^-$ groups. In compound **2**, the $[4\text{-AP}]^+$ groups exhibit a nearly parallel arrangement (Fig. 1c), similar to the $[4\text{-HP}/4\text{-H}_2\text{P}]^+$ pseudo-layers in compound **1**. In addition, π–π interactions between adjacent $[3\text{-pySO}_3]^-$ groups enhance the stability of the 2D layered structure in compound **2** (Fig. S3b†), contributing to its final configuration (Fig. 1e).

PXRD patterns (Fig. 2a and S4†) confirmed the purity of both compounds, as the experimental patterns closely match the simulated ones. IR spectra (Fig. S5a and b†) were recorded to identify characteristic vibrational peaks. For compound **1**, the [4-HP] unit exhibits peaks corresponding to $\upsilon_{C=O}$ at 1600 cm^{-1}, υ_{N-H} at 3237 cm^{-1}, υ_{S-O} at 1050 cm^{-1}, υ_{C-S} at 741 cm^{-1}, υ_{C-O} at 1298 cm^{-1}, υ_{C-H} at 818 and 840 cm^{-1}, and vibrations of $[SO_3]^-$ at 1177 cm^{-1}. In compound **2**, characteristic peaks include υ_{N-H}/υ_{py} from 1538–1671 cm^{-1}, υ_{C-S} at 746 cm^{-1}, υ_{C-H} at 809, 837, and 1020 cm^{-1}, υ_{S-O} at 1043 cm^{-1}, vibrations of $[SO_3]^-$ at 1188 cm^{-1}, and vibrations of $[NH_2]$ at 3174, 3290, and 3347 cm^{-1}.[42–45]

TGA curves (Fig. S6a and b†) indicate excellent thermal stability, with compound **1** stable up to 200 °C and compound **2**

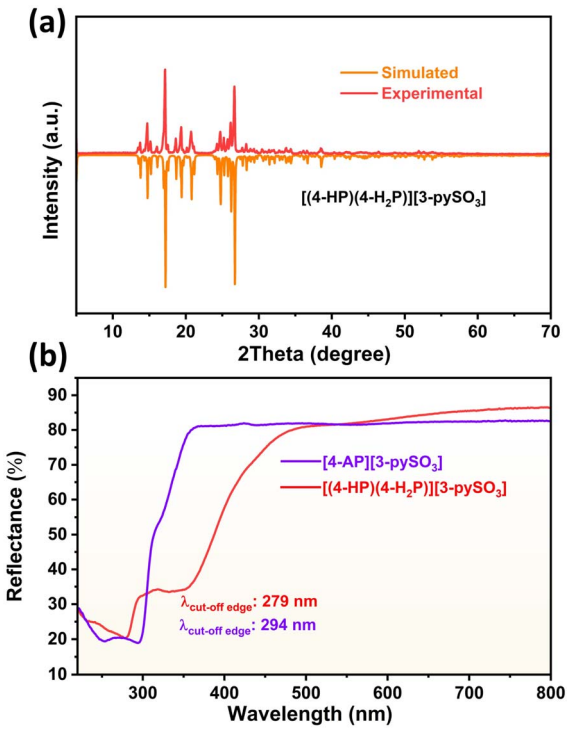

Fig. 2 (a) Simulated and experimental PXRD patterns of compound **1**; (b) UV-vis diffuse reflectance spectra of compounds **1** and **2**.

up to 217 °C. UV-vis diffuse reflectance spectra (Fig. 2b) reveal UV cut-off edges at 279 nm for compound **1** and 294 nm for compound **2**. Experimental bandgaps (Fig. S7a and b†) were determined to be 4.12 eV for compound **1** and 4.00 eV for compound **2**, suggesting both compounds are promising candidates for birefringent materials in the short-wave UV region. The cut-off edge of compound **1** is shorter than that of compound **2** because the only difference between these two compounds is the terminal groups attached to the pyridine ring: "–NH_2" in 4-AP (compound **2**) and "–OH" in 4-HP (compound **1**). Compared to "–NH_2," the "–OH" group has a stronger electron-withdrawing ability due to the higher electronegativity of oxygen compared to nitrogen. This increased electronegativity typically results in a wider transparent region, ultimately causing a blue shift in the cut-off edge.[25]

The electronic structures of compounds **1** and **2** were analyzed using first-principles DFT calculations. Calculated band structure spectra (Fig. S8a and b†) reveal direct bandgaps of 3.495 eV for compound **1** and 3.134 eV for compound **2**, with both the conduction band minimum (CBM) and valence band maximum (VBM) located at the Γ point. The discrepancy between the calculated and experimental bandgaps (4.12 eV for compound **1** and 4.00 eV for compound **2**) can be attributed to the discontinuity in the exchange-correlation energy functional when using the GGA-PBE approximation.[46–49] A scissor correction was applied in subsequent analyses.

Given the close relationship between optical properties and electronic states near the Fermi level (0 eV), the DOS was calculated (Fig. 3a and b). For compound **1**, the VBM and CBM are primarily derived from C-2p in both $[4\text{-}H_2P]^+$/[4-HP] and $[3\text{-}pySO_3]^-$ groups, N-2p as well as O-2p orbitals, with minor contributions from N-2s, H-1s, and S-3p at the VBM, and S-3p and H-1s at the CBM. Similarly, in compound **2**, the VBM is dominated by C-2p in both $[4\text{-}AP]^+$ and $[3\text{-}pySO_3]^-$ groups, N-2p as well as O-2p orbitals, with minor contributions from N-2s, H-1s, and S-3p, while the CBM is primarily composed of C-2p and N-2p orbitals. The prominence of C-2p and N-2p orbitals at the CBM in compound **2** is attributed to the substitution of the "–OH" group with "–NH_2," which alters the electronic structure.

The primary contributors to the optical properties of both compounds are the $[4\text{-}H_2P]^+$/[4-HP], $[4\text{-}AP]^+$, and $[3\text{-}pySO_3]^-$ groups.[50–52] To further explore the distribution of electron density around these groups, ELF calculations were performed (Fig. 3c and d for compound **1**; Fig. S9a and b† for compound **2**). The ELF results reveal distorted electron cloud shapes, indicating synergistic effects between the π-conjugated units. These effects contribute to the significant optical anisotropy observed in compounds **1** and **2**, thereby enhancing birefringence.[53–55]

Birefringence was further calculated using first-principles methods. As shown in Fig. 4, compounds **1** and **2** exhibit excellent birefringence values of 0.446 and 0.312 at 546 nm, respectively, both exceeding 0.3. The birefringence of compounds was also measured experimentally using a ZEISS Axiolab 5 polarizing microscope, following the formula $\Delta n = R/d$. Complete extinction was achieved for compound **1** (Fig. 4) and compound **2** (Fig. 5). The optical path difference (R) values were determined to be 3.107 and 3.488 at 546 nm for compounds **1** and **2**, respectively, with corresponding crystal thicknesses (d) of 7 and 11.787 μm (Fig. 4b, 5d; S10 and S11†). Consequently, the experimental birefringence values of 0.443 for compound **1** and 0.296 for compound **2** closely align the calculated values, confirming the reliability of the CASTEP calculations.

Notably, these birefringence values surpass those of commercial birefringent crystals, such as TiO_2 (0.305 @546 nm), YVO_4 (0.225 @633 nm), $CaCO_3$ (0.172 @589 nm), and $LiNbO_3$ (0.074 @546 nm) (Table S9†). The birefringence of compound **1** represents the highest value reported among UV-active sulfate derivatives incorporating additional BAGs (Fig. 4f, Table S8†). The $[3\text{-}pySO_3]^-$ unit, identified as an

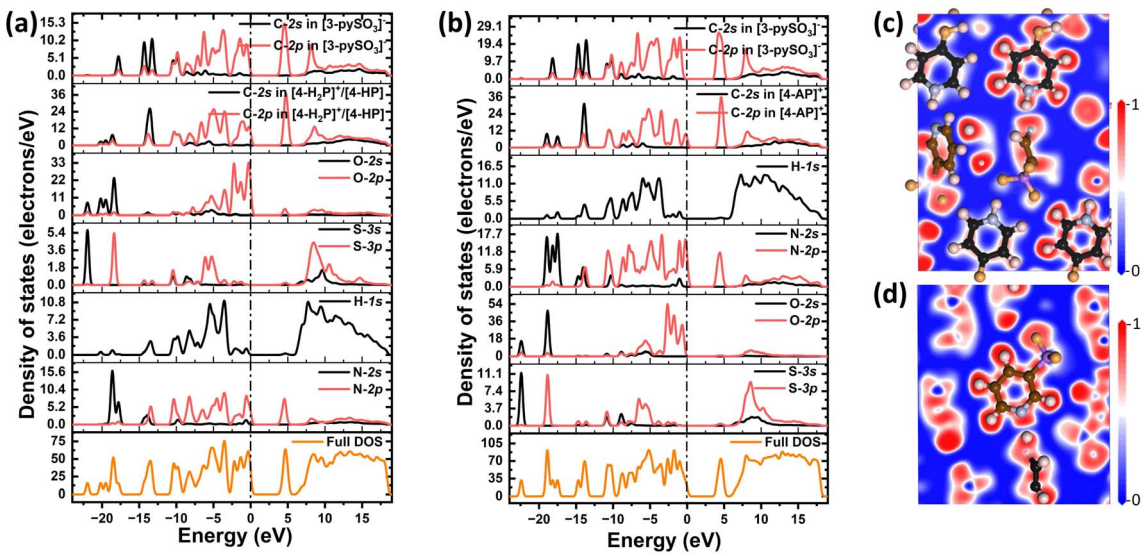

Fig. 3 Calculated density of states of (a) compound **1** and (b) compound **2**; calculated ELF diagrams of (c) $[4\text{-}H_2P]^+$/[4-HP] and (d) $[3\text{-}pySO_3]^-$ groups in compound **1**.

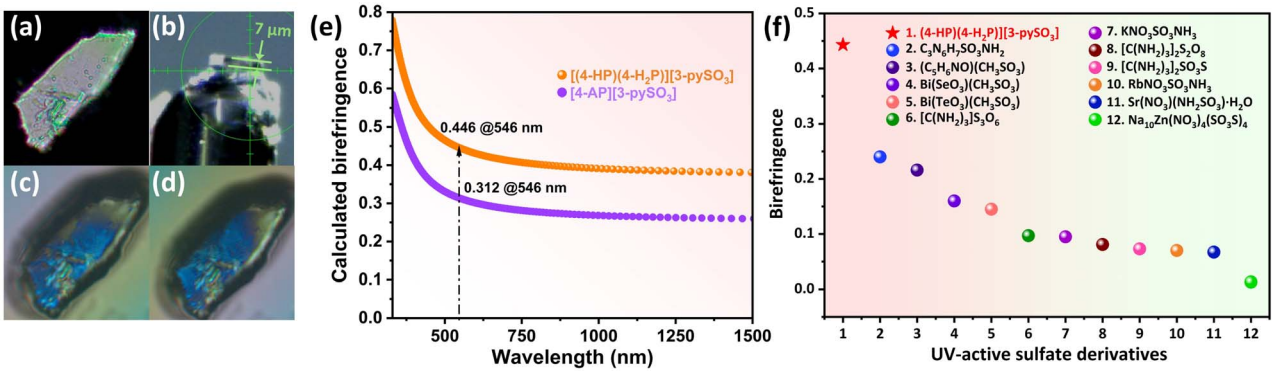

Fig. 4 (a) Crystal of compound **1** under cross-polarized light; (b) thickness of compound **1** crystal used for birefringence measurement; (c and d) crystal of compound **1** achieving complete extinction under a polarizing microscope; (e) calculated birefringence at 546 nm for compounds **1** and **2**; (f) experimental birefringence values of UV-active sulfate derivatives incorporating an additional BAG, including compound **1** (red star). More details are provided in Table S8.†

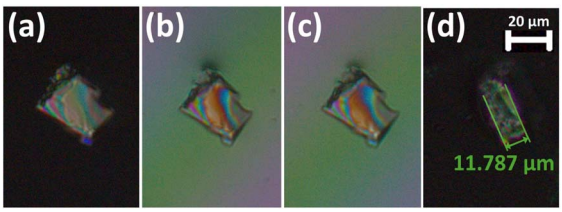

Fig. 5 (a) Crystal of compound **2** under cross-polarized light; (b and c) crystal of compound **2** achieving complete extinction under a polarizing microscope; (d) thickness of the compound **2** crystal used for birefringence measurement.

excellent BAG, was further explored in a series of compounds, $A(3\text{-}pySO_3)\cdot xH_2O$ (A = Ag, NH_4, and alkali metals).[56] In these compounds, the dihedral angle of the $[3\text{-}pySO_3]^-$ group in $Li(3\text{-}pySO_3)\cdot H_2O$ (62.11°) is comparable to that in compound **1** (64.06°) (Fig. S12a and b†). In $Li(3\text{-}pySO_3)\cdot H_2O$, the contribution of $[LiO_4]$ tetrahedra to birefringence is limited, with the primary contribution coming from the birefringence-active group $[3\text{-}pySO_3]^-$. The density of $[3\text{-}pySO_3]^-$ was calculated as $\rho = 4/768.24 = 5.21 \times 10^{-3}$ Å^{-3}. In compound **1**, two types of birefringence-active groups (BAGs) are present. Consequently, the density of BAGs (ρ_{BAGs}) increases from 5.21×10^{-3} Å^{-3} to 7.55×10^{-3} Å^{-3} with the introduction of well-aligned $[4\text{-HP/4-}H_2P]^+$ pseudo-layers. This results in a 70% increase in birefringence, from $\Delta n = 0.26$ in $Li(3\text{-}pySO_3)\cdot H_2O$ to $\Delta n = 0.443$ in compound **1**. Furthermore, compound **1** also demonstrates the highest birefringence among metal-free compounds containing single 6-MRs in the short-wave UV region (Fig. 6, Table S7†).

Although compounds **1** and **2** share similar chemical compositions, they exhibit distinct birefringent optical properties, primarily due to the differences in their terminal groups, "–NH_2" and "–OH" found in 4-AP and 4-HP, respectively. In compound **2**, the "–NH_2" group is inherently restricted to acting as a hydrogen bond donor, forming single monovalent $[4\text{-AP}]^+$ cations with protonation of the nitrogen atom in the pyridine ring. In contrast, the "–OH" group in compound **1** can act as both a hydrogen bond donor and acceptor due to its potential for deprotonation. This dual functionality facilitates the formation of unique $[4\text{-HP/4-}H_2P]^+$ dimer pairs in compound **1**, linked *via* O–H···O hydrogen bonds to achieve charge balance within the structure. As a result, two-thirds of the cationic groups in compound **1** align uniformly, occupying the entire structure, whereas only half of the cationic groups in compound **2** exhibit a nearly parallel alignment. This distinction results in a greater degree of optical anisotropy in compound **1**. Specifically, the density of $[4\text{-HP/4-}H_2P]^+$ is calculated to be 5.04×10^{-3} Å^{-3}, compared to 3.38×10^{-3} Å^{-3} for $[4\text{-AP}]^+$, representing a 49% increase from compound **2** to compound **1**. In contrast, the density of $[3\text{-}pySO_3]^-$ in the two compounds is relatively similar (3.38×10^{-3} Å^{-3} in compound **2** *vs.* 2.52×10^{-3} Å^{-3} in compound **1**). This variation appears to enhance the denser spatial distribution of pyridine primitives in the unit cell, particularly within the cationic groups.

Furthermore, the transition from $[4\text{-AP}]^+$ to $[4\text{-HP/4-}H_2P]^+$ dimer pairs alters the overall structure, influencing the arrangement of the anionic $[3\text{-}pySO_3]^-$ groups. The dihedral angle between the pyridine ring in $[3\text{-}pySO_3]^-$ and the cationic groups decreases from 71.82° in compound **2** to 56.98° in compound **1** (Fig. S13a and b†). As previously analyzed in $C(NH_2)_3CH_3SO_3$, the larger polarizability tensorial components

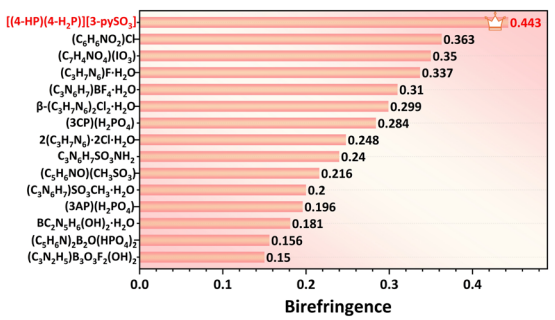

Fig. 6 Experimental birefringence of metal-free compounds containing single 6-MRs in the short-wave UV region, including compound **1**. More details are provided in Table S7.†

of the coplanar $[C(NH_2)_3]^+$ unit primarily lie in the *x*, *y*, *z* plane, overlapping well with the plane formed by its C/N atoms. Therefore, it can be speculated that the larger polarizability direction is predominantly distributed within the pyridine ring planes of $[4\text{-AP}]^+$, $[4\text{-H}_2\text{P}]^+$, $[3\text{-pySO}_3]^-$, and neutral [4-HP]. In contrast, for $[CH_3SO_{33}]^-$, the polarizability is nearly perpendicular to that of $[C(NH_2)_3]^+$, which negatively affects birefringence. Thus, the smaller dihedral angle between the pyridine cations and anions in compounds **1** and **2** positively contributes to birefringence. Additionally, reduction in structural dimensionality from supramolecular 2D $[4\text{-AP}(3\text{-pySO}_3)]_\infty$ layers in compound **2** to supramolecular 1D $[(4\text{-HP})(4\text{-H}_2\text{P})][3\text{-pySO}_3]_\infty$ chains in compound **1** also contributes to the observed increase in birefringence.[57,58]

Conclusions

In conclusion, distinct pyridine derivatives were successfully integrated into single structures to create two novel UV metal-free crystals: the supramolecular 1D compound $[(4\text{-HP})(4\text{-H}_2\text{P})][3\text{-pySO}_3]$ (**1**) and 2D compound $[4\text{-AP}][3\text{-pySO}_3]$ (**2**). These crystals were synthesized using a mild aqueous solution method. Both compounds exhibit significant birefringence, with values of 0.443 and 0.296 at 546 nm for compounds **1** and **2**, respectively, driven by differences in the composition and arrangement of organic cations. Specifically, compound **1** features unique $[4\text{-HP}/4\text{-H}_2\text{P}]^+$ cationic dimer pairs linked by hydrogen bonds, in contrast to the single monovalent $[4\text{-AP}]^+$ cations in compound **2**. This arrangement enhances the alignment of anionic $[3\text{-pySO}_3]^-$ groups, reduces the dimensionality of the linking mode, and increases the density of $[4\text{-HP}/4\text{-H}_2\text{P}]^+$ pseudo-layers, ultimately boosting the birefringence. First-principles calculations confirm the synergistic effects between the cationic and anionic pyridine derivatives in enhancing birefringence. With its high birefringence, short UV cut-off edge of 279 nm, and favorable growth characteristics, compound **1** demonstrates significant potential as a UV birefringent crystal. This research provides new insights into the designing birefringent crystals by optimizing the relationship between the composition and configuration of organic cations and their optical properties in UV metal-free systems through synergistic effects.

Data availability

The data that support the findings of this study are available from the corresponding author, KMO, upon reasonable request.

Author contributions

K. M. O. initiated the project and secured funding for the research. J. L. conducted the experimental work. Both J. L. and K. M. O. contributed to writing the manuscript and approved the final version.

Conflicts of interest

There are no conflicts to declare.

Acknowledgements

This research was supported by the National Research Foundation of Korea (NRF) funded by the Ministry of Science and ICT (Grant No. RS-2024-00442105).

Notes and references

1 J. W. Evans, *J. Opt. Soc. Am.*, 1949, **39**, 229–242.
2 M. Li, H. Pan, Y. Tong, C. Chen, Y. Shi, J. Wu and H. Zeng, *Opt. Lett.*, 2011, **36**, 3633–3635.
3 F. Flossmann, U. T. Schwarz, M. Maier and M. R. Dennis, *Phys. Rev. Lett.*, 2005, **95**, 253901.
4 P. Hlubina, D. Ciprian and L. Knyblova, *Opt. Commun.*, 2006, **260**, 535–541.
5 L. H. Nicholls, F. J. Rodríguez-Fortuño, M. E. Nasir, R. M. Córdova-Castro, N. Olivier, G. A. Wurtz and A. V. Zayats, *Nat. Photonics*, 2017, **11**, 628–633.
6 H. Fan, M. Ryu, R. Honda, J. Morikawa, Z. Z. Li, L. Wang, J. Maksimovic, S. Juodkazis, Q. D. Chen and H. B. Sun, *Nanomaterials*, 2019, **9**, 1414.
7 J. R. DeVore, *J. Opt. Soc. Am.*, 1951, **41**, 416–419.
8 H. Luo, T. Tkaczyka, R. Sampsonb and E. L. Dereniaka, *Semicond. Photodetectors III*, 2006, vol. 6119, pp. 136–142.
9 D. E. Zelmon, D. L. Small and D. Jundt, *J. Opt. Soc. Am. B*, 1997, **14**, 3319–3322.
10 X. Chen, B. Zhang, F. Zhang, Y. Wang, M. Zhang, Z. Yang, K. R. Poeppelmeier and S. Pan, *J. Am. Chem. Soc.*, 2018, **140**, 16311–16319.
11 W. Huang, X. Zhang, Y. Li, Y. Zhou, X. Chen, X. Li, F. Wu, M. Hong, J. Luo and S. Zhao, *Angew. Chem., Int. Ed.*, 2022, **61**, e202202746.
12 Y. Shen, L. Ma, G. Dong, H. Yu and J. Luo, *Inorg. Chem. Front.*, 2023, **10**, 2022–2029.
13 Y. Li, X. Chen and K. M. Ok, *Chem. Sci.*, 2024, **15**, 15145–15151.
14 Y. Zhao, C.-L. Hu, P.-F. Chen, M.-Z. Zhang and J.-G. Mao, *CrystEngComm*, 2024, **27**, 30–37.
15 Y. Deng, L. Wang, Y. Ge, L. Huang, D. Gao, J. Bi and G. Zou, *Chem. Commun.*, 2020, **56**, 9982–9985.
16 Y. Shen, Y. Zhou, X. Xue and G. Dong, *Inorg. Chem.*, 2023, **62**, 8482–8486.
17 X. Zhang, B. Xu, D. Xiao, L. Dong, X. Zhang, P. Gong and Z. Lin, *Inorg. Chem.*, 2024, **63**, 17907–17913.
18 M. Mutailipu, J. Han, Z. Li, F. Li, J. Li, F. Zhang, X. Long, Z. Yang and S. Pan, *Nat. Photonics*, 2023, **17**, 694–701.
19 C. Jin, F. Li, Z. Yang, S. Pan and M. Mutailipu, *J. Mater. Chem. C*, 2022, **10**, 6590.
20 Z.-P. Zhang, X. Liu, X. Liu, Z.-W. Lu, X. Sui, B.-Y. Zhen, Z. Lin, L. Chen and L.-M. Wu, *Chem. Mater.*, 2022, **34**, 1976–1984.
21 Q. Q. Chen, C. L. Hu, M. Z. Zhang and J. G. Mao, *Chem. Sci.*, 2023, **14**, 14302–14307.

22 M.-B. Xu, Q.-Q. Chen, B.-X. Li, K.-Z. Du and J. Chen, *Chin. Chem. Lett.*, 2024, DOI: **10.1016/j.cclet.2024.110513**.
23 J. P. Yin, J. Guo, H. Huo, X. Liu, X. J. Cheng, Z. Lin, L. M. Wu and L. Chen, *Angew. Chem., Int. Ed.*, 2024, e202417579, DOI: **10.1002/anie.202417579**.
24 M. Xia, M. Mutailipu, F. Li, Z. Yang and S. Pan, *Cryst. Growth Des.*, 2021, **21**, 1869–1877.
25 Y. Shen, M. Ding, G. Chen, Y. Luo, S. Zhao and J. Luo, *Small*, 2024, **20**, e2400549.
26 X. Meng, F. Liang, K. Kang, J. Tang, Q. Huang, W. Yin, Z. Lin and M. Xia, *Dalton Trans.*, 2019, **48**, 9048–9052.
27 M. Li, X. Zhang, Z. Xiong, Y. Li, Y. Zhou, X. Chen, Y. Song, M. Hong, J. Luo and S. Zhao, *Angew. Chem., Int. Ed.*, 2022, **61**, e202211151.
28 Y. Li, X. Zhang, Y. Zhou, W. Huang, Y. Song, H. Wang, M. Li, M. Hong, J. Luo and S. Zhao, *Angew. Chem., Int. Ed.*, 2022, **61**, e202208811.
29 Y. Zhao, L. Zhu, Y. Li, X. Kuang, J. Luo and S. Zhao, *Mater. Chem. Front.*, 2023, **7**, 3986–3993.
30 F. Liang, L. Kang, X. Zhang, M.-H. Lee, Z. Lin and Y. Wu, *Cryst. Growth Des.*, 2017, **17**, 4015–4020.
31 SAINT, *version 7.60A, Bruker Analytical X-Ray Instruments Inc.*, Madison, WI, 2008.
32 O. V. Dolomanov, L. J. Bourhis, R. J. Gildea, J. A. K. Howard and H. Puschmann, *J. Appl. Crystallogr.*, 2009, **42**, 339–341.
33 A. L. Spek, *J. Appl. Crystallogr.*, 2003, **36**, 7–13.
34 S. J. Clark, M. D. Segall, C. J. Pickard, P. J. Hasnip, M. I. J. Probert, K. Refson and M. C. Payne, *Z. Kristallogr. – Cryst. Mater.*, 2005, **220**, 567–570.
35 W. Wang, H. Fan and Y. Ye, *Polymer*, 2010, **51**, 3575–3581.
36 J. Lin, A. Qteish, M. C. Payne and V. Heine, *Phys. Rev. B:Condens. Matter Mater. Phys.*, 1993, **47**, 4174.
37 J. P. Perdew, K. Burke and M. Ernzerhof, *Phys. Rev. Lett.*, 1996, **77**, 3865–3868.
38 K. Liu, H. Fan, P. Ren and C. Yang, *J. Alloys Compd.*, 2011, **509**, 1901–1905.
39 X. Zhang, X. Du, J. Wang, F. Wang, F. Liang, Z. Hu, Z. Lin and Y. Wu, *ACS Appl. Mater. Interfaces*, 2022, **14**, 53074–53080.
40 Z. Chen, Q. Wu, J. Hong, G. Dong and L. Ma, *J. Mater. Chem. C*, 2024, **12**, 5696–5700.
41 D. Dou, Q. Shi, H. Li, B. Zhang, D. Yang and Y. Wang, *Adv. Sci.*, 2024, **11**, e2401325.
42 J. Lu, X. Liu, M. Zhao, X. B. Deng, K. X. Shi, Q. R. Wu, L. Chen and L. M. Wu, *J. Am. Chem. Soc.*, 2021, **143**, 3647–3654.
43 P. Purushothaman, R. Gopathy, E. Raju, N. Durairaj, S. Kandhan and G. Mani, *J. Mater. Sci.:Mater. Electron.*, 2021, **32**, 22342–22361.
44 Y. Li and K. M. Ok, *Chem. Sci.*, 2024, **15**, 10193–10199.
45 Z. P. Zhang, X. Liu, R. X. Wang, S. Zhao, W. J. He, H. Y. Chen, X. B. Deng, L. M. Wu, Z. Zhou and L. Chen, *Angew. Chem., Int. Ed.*, 2024, **63**, e202408551.
46 T. Wu, X. Jiang, Y. Zhang, Z. Wang, H. Sha, C. Wu, Z. Lin, Z. Huang, X. Long, M. G. Humphrey and C. Zhang, *Chem. Mater.*, 2021, **33**, 9317–9325.
47 H. Zhou, M. Cheng, D. Chu, X. Liu, R. An, S. Pan and Z. Yang, *Angew. Chem., Int. Ed.*, 2024, e202413680, DOI: **10.1002/anie.202413680**.
48 Y. Chen, H. Luo, Z. Yin, X. Dong, D. Gao, Y. Zhou, L. Huang, L. Cao and G. Zou, *Inorg. Chem.*, 2024, **63**, 15206–15214.
49 J. Lv, G. Yi, X. Zou, H. Liu, X. Han, L. Huang, H. Zeng, Z. Lin and G. Zou, *Chem. Mater.*, 2024, **36**, 12018–12025.
50 Y. Li and K. M. Ok, *J. Mater. Chem. C*, 2022, **10**, 8776–8782.
51 X. Du, F. Wang, F. Liang, Z. Hu, Y. Wu and X. Zhang, *Inorg. Chem. Front.*, 2023, **10**, 5979–5985.
52 S. Ke, H. Fan, C. Lin, N. Ye and M. Luo, *Inorg. Chem. Front.*, 2023, **10**, 2811–2817.
53 J. Guo, A. Tudi, S. Han, Z. Yang and S. Pan, *Angew. Chem., Int. Ed.*, 2019, **58**, 17675–17678.
54 Y. Li, X. Zhang, J. Zheng, Y. Zhou, W. Huang, Y. Song, H. Wang, X. Song, J. Luo and S. Zhao, *Angew. Chem., Int. Ed.*, 2023, **62**, e202304498.
55 X. Wang, Y. Li, Z. Chen, J. Lee, F. Zhang, K. R. Poeppelmeier, S. Pan and K. M. Ok, *Small Struct.*, 2023, **4**, 2300274.
56 Z. Bai and K. M. Ok, *Angew. Chem., Int. Ed.*, 2024, **63**, e202315311.
57 Q. Xu, W. Huang, H. Wang, Y. Li, Y. Zhou, L. Hou, S. Zhao and J. Luo, *Small*, 2023, **19**, e2304333.
58 Y. Li and K. M. Ok, *Angew. Chem., Int. Ed.*, 2024, **63**, e202409336.